

An Ultrafast and Post-Treatment Free Method of Zinc Oxide Nanoparticles Synthesis Using Anodic Oxidation

Christophe Massard^{1,2}, Vincent Raspal^{1,2}, Christelle Blavignac³, Claire Szczepaniak³, Komla Oscar Awitor^{1,2}

¹Laboratoire de physique de Clermont Auvergne (LPCA), Université Clermont Auvergne, Pôle santé et Environnement, Clermont-Ferrand, France

²Equipe Physico-Chimie des Surfaces Nanostructurées (P.C.S.N), Institut Universitaire de Technologie Clermont-Ferrand, Aubière, France

³Centre d'Imagerie Cellulaire Santé (CICS), Université Clermont-Auvergne, Clermont-Ferrand, France

Email: christophe.massard@uca.fr

How to cite this paper: Massard, C., Raspal, V., Blavignac, C., Szczepaniak, C. and Awitor, K.O. (2025) An Ultrafast and Post-Treatment Free Method of Zinc Oxide Nanoparticles Synthesis Using Anodic Oxidation. *Advances in Nanoparticles*, 14, 73-90.

<https://doi.org/10.4236/anp.2025.143005>

Received: April 11, 2025

Accepted: June 24, 2025

Published: June 27, 2025

Copyright © 2025 by author(s) and Scientific Research Publishing Inc.

This work is licensed under the Creative Commons Attribution International License (CC BY 4.0).

<http://creativecommons.org/licenses/by/4.0/>



Open Access

Abstract

Zinc oxide (ZnO) nanoparticles are easily prepared from zinc solid using an electrochemical technique. A quick anodic oxidation under constant voltage of a zinc foil in an aqueous potassium chloride electrolyte leads to the fabrication of ZnO nanoparticles in a single-step process at room temperature and without the use of controversial chemical reagents. The crystallographic structure of the fabricated nanoparticles is characterized using X-ray diffraction (XRD) spectroscopy. Field emission scanning electron microscopy (FESEM) and transmission electron microscopy (TEM) are used to reveal the morphology and aggregate size of the nanopowder. The energy dispersive spectra obtained from the SEM-EDS confirm that the sample prepared is in the ZnO phase. The photocatalytic property of the synthesized ZnO nanoparticles is evaluated in studying the degradation of the Acid orange 7 (AO7) organic dye in the presence of the ZnO nanoparticles as a catalyst under UV-visible irradiation.

Keywords

Zinc Oxide Nanoparticles, Nanopowder, Anodic Oxidation, Photocatalysis

1. Introduction

Since the mid-1960s, following the pioneering research of Peter Speiser [1], nanoparticles have attracted growing interest. The properties of finely divided matter

offer a wealth of opportunities for discovery [2]. Innovative technological applications can be envisaged by the development of nanotechnology [3]. Among all the kinds of nanomaterials, nanoparticles are considered as building blocks of primary importance [4]. Numerous fields of applications from biology and medicine [5] [6], industrial [7]-[9] agriculture [10] [11] to environmental [12] and space applications [13] [14] are concerned. To develop these applications, nanoparticle production is of prime importance, including various top-down [15] and bottom-up approaches [16]. Among the many particles produced, ZnO nanoparticles are highly attractive considering their wide band gap [17], very suitable for optoelectronics applications [17]-[19] and solar cell devices [20]-[22]. Different synthesis methods are commonly used to produce ZnO nanoparticles including direct precipitation [23]-[25], sol-gel techniques [26]-[28], hydrothermal process [29]-[31], spray pyrolysis [32]-[34] for the most common ones, these approach need thermal post treatment to achieve a suitable crystallinity of the final products [35]-[37]. On the other hand, electrochemical anodization processes are mainly dedicated to the surface modification of bulk material [38]-[41], also called nanostructure formation. Few studies focus on the synthesis of nanoparticles using the anodization technique. In this paper, we elaborate on ZnO nanoparticles by chemical anodizing a Zn foil. This unusual synthesis method produces, in a few seconds, a large amount of ZnO nanoparticles and doesn't require any thermal post-treatment. This method doesn't require controversial chemical reagents or time-consuming steps.

2. Materials and Methods

2.1. Anodization Set-Up

The anodization setup is a custom-built apparatus (**Figure 1**). It includes a TDK[®] Lambda GENH300-2.5 DC power supply, which serves as the voltage generator, and an Agilent[®] 34401A multimeter for data recording during experiments. These instruments are interfaced with a computer. The lab has developed software named Nanobuilder to control the electrochemical cell via a GPIB interface, utilizing LabVIEW 8[®] from National Instruments[®] as the systems engineering tool. Nanobuilder regulates the target voltage applied to the anodizing cell by following a predefined voltage profile. Throughout the process, the generator provides feedback on the actual voltage applied, while the ammeter measures the anodizing current. The software logs these values in a file for real-time monitoring and subsequent analysis.

2.2. Sample Preparation

All chemicals are used without any post-treatment. Potassium chloride electrolyte solution 0.2 M is prepared by weighing and dissolving the appropriate amount of KCl (Fisher Chemical[®]) in deionized water. We used zinc foil with a purity of 99.7% (Goodfellow[®] England) and a thickness of 1 mm as starting material. A ribbon 5.5 cm long by 1 cm wide is cut from the zinc plate to form the anode. The

zinc ribbon is degreased and cleaned by successive sonication in a series of baths during 5 minutes at each step: trichloroeth-ylene (Acros Organics®), acetone (Fisher Chemical®), ethanol (Prolabo®) and deionized water are successively used to ensure a good surface finish prior to the anodization step. The zinc electrode is finally blown dry with dry air.

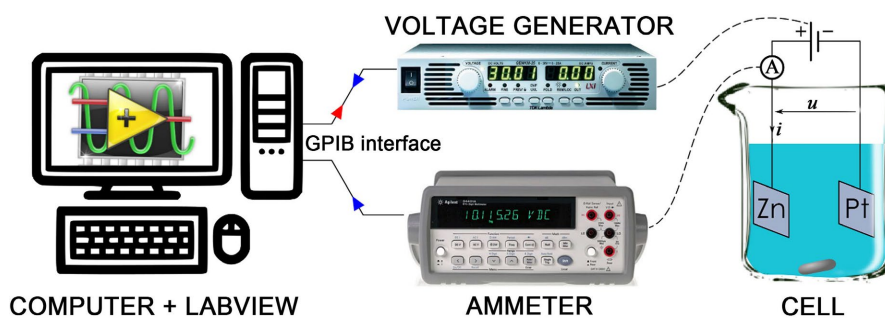


Figure 1. Schematic representation of the custom-built anodization setup.

2.3. Fabrication of ZnO Nanoparticles by Anodization of Zn Foil

The electrochemical cell is a classical electrolysis system consisting of a Pt foil as counter-electrode (cathode) and the zinc ribbon as the working electrode (anode). During the experiments, the stirring speed is kept constant (180 rpm). The zinc foil is anodized at room temperature under a constant voltage of 12 V. Anodization transforms the zinc foil into metal oxide nanoparticles. The process stops when the zinc bar is completely dissolved, thus opening the circuit. The produced nanoparticles are collected, separated from the electrolyte by centrifugation (artificial gravity acceleration: 100 g) and washed many times with deionized water to remove undesired salt incorporated during the anodization.

2.4. Pycnometer Density Method

The density of the produced powder is evaluated using the pycnometer method. The density of the xylene isomer blend (Fisher Chemical®) is used as reference. All the adjustments are made at room temperature.

The method consists of a series of high-precision weighing operations:

m_1 is the mass of the empty pycnometer;

m_2 is the mass of the pycnometer filled with water;

m_3 is the mass of the pycnometer filled with xylene;

m_4 is the mass of the pycnometer containing 1 gram of powder;

m_5 is the mass of the pycnometer containing the powder and filled with xylene.

For this last measurement, the powder is immersed in xylene and degassed under vacuum and ultrasound for at least 10 minutes and 5 minutes, respectively. Then the adjustment with xylene is finished. As a consequence, the density expressions are the following:

$$d_{\text{xylene}} = \frac{m_3 - m_1}{m_2 - m_1} \times d_{\text{water}} \quad (1)$$

$$d_{\text{powder}} = \frac{m_4 - m_1}{(m_3 - m_1) - (m_5 - m_4)} \times d_{\text{xylen}} \quad (2)$$

2.5. X-Ray Diffraction Spectroscopy

The crystal structure of the produced ZnO nanoparticles is investigated by Bruker® D2 Phaser diffractometer using CuK α 1 at 1.5406 Å with a nickel filter. The data are collected in a range that covers 2θ from 20° to 80°. The dried nanopowder of ZnO is ground before analysis with an agate mortar and pestle.

2.6. Field Emission Scanning Electron Microscopy & Energy Dispersive X-Ray Spectroscopy

Observations are carried out using a field emission scanning electron microscope Regulus 8230 (Hitachi®, Japan) at 2 kV with the secondary electron detector.

ZnO powder is deposited on stubs using adhesive carbon tabs and coated with platinum (Quorum® Q150 TES, UK). For microanalysis using energy dispersive X-ray spectroscopy, an acceleration tension at 15 kV is used with the Ultim Max® 170 mm² detector and AZtech® software (Oxford, UK).

2.7. Transmission Electron Microscopy

TEM pictures are obtained using an 80 kV transmission electron microscope (Hitachi® H-7650) with Hamamatsu® camera AMT 40 (4k). ZnO powder was dispersed in distilled water. 40 µL of this dispersion is spread on a Nickel formvar-carbon grid.

2.8. Photocatalytic Test of the ZnO Nanoparticles

A 50 mL aqueous solution of 40 ppm Acid Orange 7 (Acros Organics®) dye is prepared.

40 mg of dried ZnO nanopowder is suspended in the solution dye under stirring. The suspension is ultra-sonicated for 30 minutes in the dark to ensure a sufficient homogeneity of the medium as well as to reach the adsorption equilibrium. A homemade photo-reactor equipped with six 8-W low-pressure mercury vapor tubular lamps, a magnetic stirrer and a fan is used to perform the analysis. A control is made by measuring the absorbance of the dye solution in the same irradiator and over the same time as was made first. The absence of any change in absorbance after irradiation shows that radiation alone could not degrade the dye. The pH of the AO7 solution during the photocatalytic experiments is adjusted to 6. A 5 mL aliquot is taken out of the quartz reactor beaker at regular intervals, followed by centrifugation at 100 g for 5 minutes to separate ZnO nanoparticles from the AO7 solution. Each supernatant is analyzed using a Jenway® model 7310 single-beam spectrophotometer. Permuted water ensures the blank. Spectral analyses are carried out between 300 and 700 nm wavelengths. Considering the AO7 dye, the maximum absorbance peak corresponds to a 486 nm wavelength. At the maximum absorbance wavelength, the percentage photocatalytic degradation is

calculated using Equation (3).

$$\text{Photodegradation (\%)} = \frac{A_0 - A_t}{A_0} \quad (3)$$

where A_0 is the initial maximum absorbance of the solution AO7, and A_t is the absorbance after a defined irradiation time t .

3. Results and Discussions

3.1. ZnO Nanoparticles Formation Process

When the DC power supply is switched on between the electrodes, instantaneously, the metallic zinc (anode) starts to be converted into metal oxide nanoparticles. The KCl electrolyte becomes instantly cloudy, and simultaneously, dihydrogen (H₂) bubbles are emitted at the Pt surface (cathode). A rapid electrochemical reaction occurs, considering the high gas flow at the cathode. The anodization curve is plotted in **Figure 2**. This anodizing current versus time curve is totally different from the well-known curves relative to the formation of nanotubular structure via anodization in fluoride electrolyte [42]. In these as-mentioned cases, an initial sudden decrease in anodic current is the consequence of the building of an insulating anodic oxide layer: the ionic diffusion across this layer is reduced. A few times later, the anodic current starts to increase: it is the etching of the oxide layer. After this second step, etching and oxide formation reaction compete, leading to a steady state current flow [43].

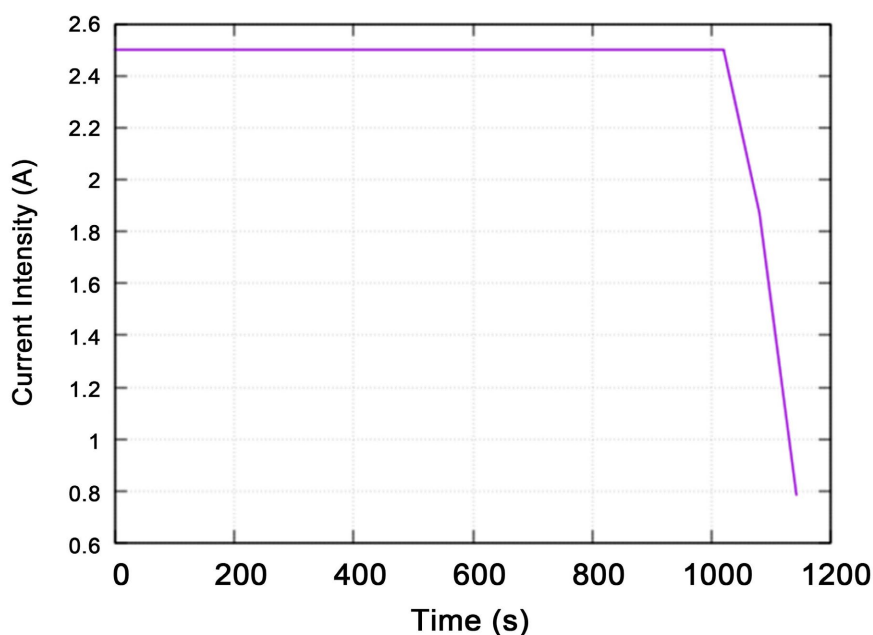
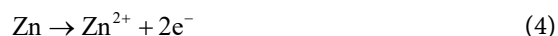


Figure 2. Current-time curve of the ZnO nanoparticles formed in 0.2 M KCl electrolyte solution under 12 V anodic voltage.

In the present experiment, a constant high current of about 2.5 A is recorded all along the anodization, attesting to the continuous dissolution of the sacrificial

zinc anode without the building of an insulating oxide layer, contrary to the usual nanotubular synthesis.

During the process, the atoms at the surface of zinc anode lose their peripheral electrons and become oxidized, following Equation (4):



Anodic cation production is continuous during the applied voltage; the repulsive electrostatic force at the metallic surface between two positively charged particles leads to a drift in the electrolyte of the cathodic species and avoids the building of an insulating oxide layer. Simultaneously, numerous gas bubbles appear on the surface of the platinum cathode, dihydrogen is produced from the electrolysis of water following Equation (5) [44]:



The metal oxide nanoparticles are synthesized when metal cation reacts with the oxygen anions following the pathway described in Equations (6) and (7) [45] [46]:



After about 16 minutes of treatment, the current drops to zero, as a result of total etching of the zinc anode, opening the circuit. The total anodizing yield depends on a number of process parameters which are currently being investigated: the most important of these are the mass of the sacrificial electrode, its surface finish, the temperature and composition of the electrolyte, the surface and type of the counter-electrode, and the applied voltage. Once all these different parameters have been established, reproducible yields require a constant level of immersion in the electrolytic bath to ensure identical production performance. Full experimental data on the influence of these parameters are not yet available and will be investigated in further studies.

3.2. Pycnometer Density Measurement

The experiments based on precision weighing of the pycnometer lead to the determination of the densities. The xylene density is found to be 0.8684 and the density of the powder is measured at 5.42. This value is different from the bulk ZnO [47]. The nanoparticulate nature of the sample as well as the measurement's parameters [48] can explain the difference found with the data in the literature [49].

3.3. X-Ray Diffraction Analysis

Figure 3 shows the X-ray diffraction pattern of the synthesized nanoparticles. Sharp peaks are observed, suggesting a well-crystallized material. The peaks at 31.773°, 34.441°, 36.262°, 47.559°, 56.604°, 62.889°, 66.388°, 67.968°, 69.097°, 72.610° and 76.978° correspond to the reflection from 100, 002, 101, 102, 210, 103, 200, 212, 201, 004, and 202 crystal planes indexed to the ZnO phase and indicate

a hexagonal zincite type crystallite with the space group P63/mc. The lattice parameters of this wurtzite type unit cell structure are $a = b = 3.24940 \text{ \AA}$ and $c = 5.20380 \text{ \AA}$.

The first peaks at the different scattering angle (2θ) are listed in **Table 1** and compared to the JCPDS card N°361451. The experimental data are consistent with the JCPDS data, and very small shifts of the experimental diffraction peaks are detected, less than 0.06% relative variation. The interplanar spacing d_{hkl} for different observed (hkl) planes is calculated using Bragg's equation:

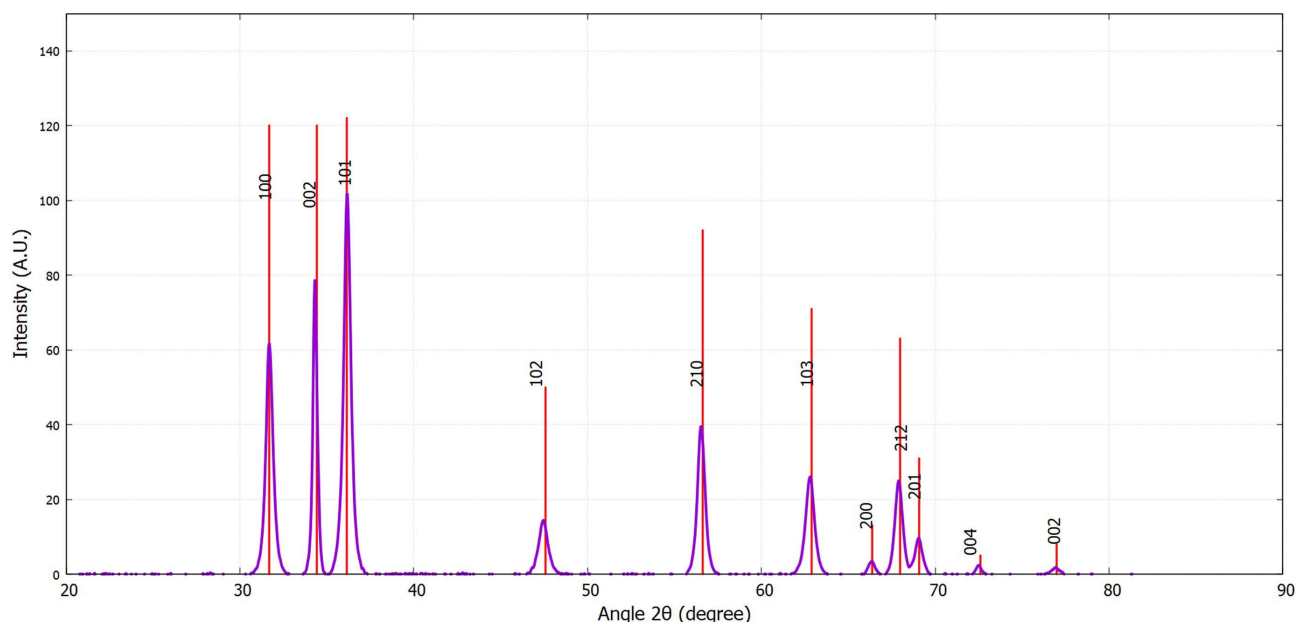


Figure 3. Experimental XRD pattern of ZnO nanoparticles obtained by anodizing Zn foil.

$$2 \times d \times \sin(\theta) = n \times \lambda \quad (8)$$

Very small differences are found between the calculated and reported values, see the calculation for the first peaks in **Table 1**.

Table 1. Comparison of the experimental XRD data with the JCPDS data (card N°361451).

(hkl) planes	Scattering angles (2θ) (degree)		$\Delta 2\theta/2\theta$ (%)	Intensity (%)		d_{hkl} (\AA)		$\Delta 2\theta/2\theta$ (%)
	JCPDS data	Experimental data		JCPDS data	Experimental data	JCPDS data	Experimental data	
(100)	31.770	31.773	0.009	57.0	59.7	2.8143	2.8114	-0.011
(002)	34.422	34.441	0.055	44.0	44.5	2.6033	2.6019	-0.006
(101)	36.253	36.262	0.025	100.0	100.0	2.4759	2.4753	-0.002
(102)	47.539	47.559	0.042	23.0	19.6	1.9111	1.9104	-0.003
(110)	56.603	56.604	0.002	32.0	35.5	1.6247	1.6247	0.000

The crystallite size is evaluated using Scherrer's equation:

$$D = \frac{K \times \lambda}{\beta \times \cos(\theta)} \quad (9)$$

D is the particle size (Å), $\lambda = 1.54056$ Å (CuK α radiation) $k = 0.94$ and β is the Full Width at half Maximum (FWHM). The crystallite size is found to be 27.7 nm.

3.4. Field Emission Scanning Electron Microscopy (FESEM) & Energy Dispersive X-Ray (EDS) Characterizations

Figure 4(a) shows the FESEM images of the produced material. The powder consists of micrometric-sized aggregates (**Figure 4(a)**). This agglomeration and clustering of the particles is an obvious result of their high surface energy [50]. Magnifications of the sample reveal a dual structure made up of micrometric grains on which nanometric crystallites are present, ranging in size from approximately 10 to 130 nm **Figure 4(b)**). These nanometric structures are designed as dots [51] [52]. These microscopic images of nanometric structures superimposed on micrometric aggregates significantly increase the specific surface area [53] [54]. The increase in specific surface area is an important parameter for catalytic applications [55] [56].

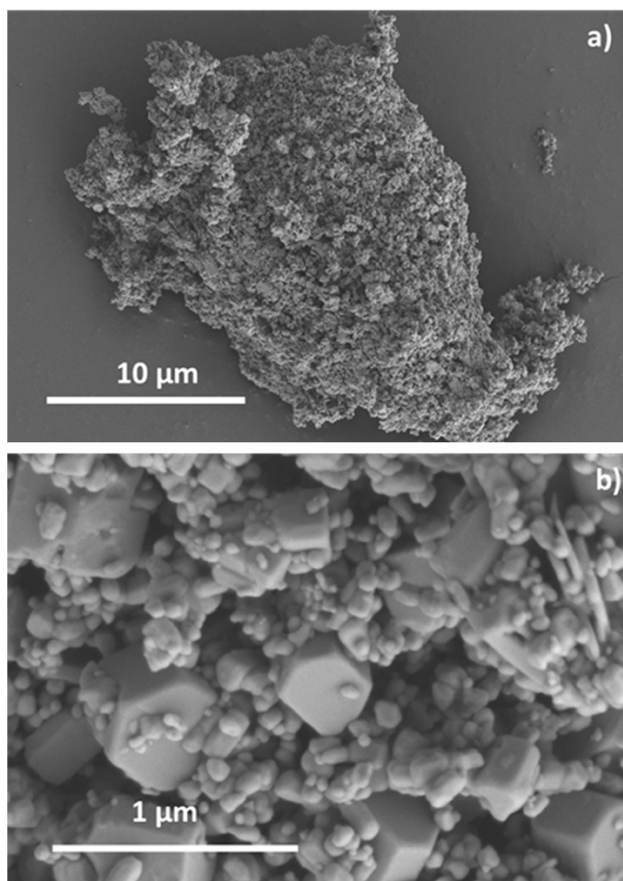
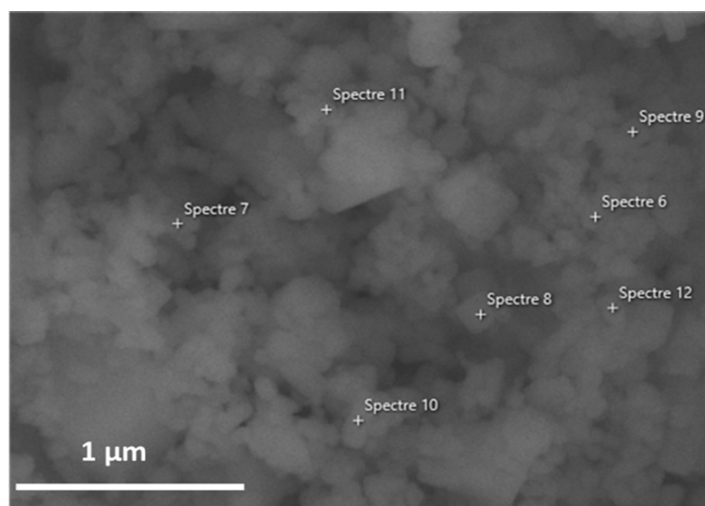


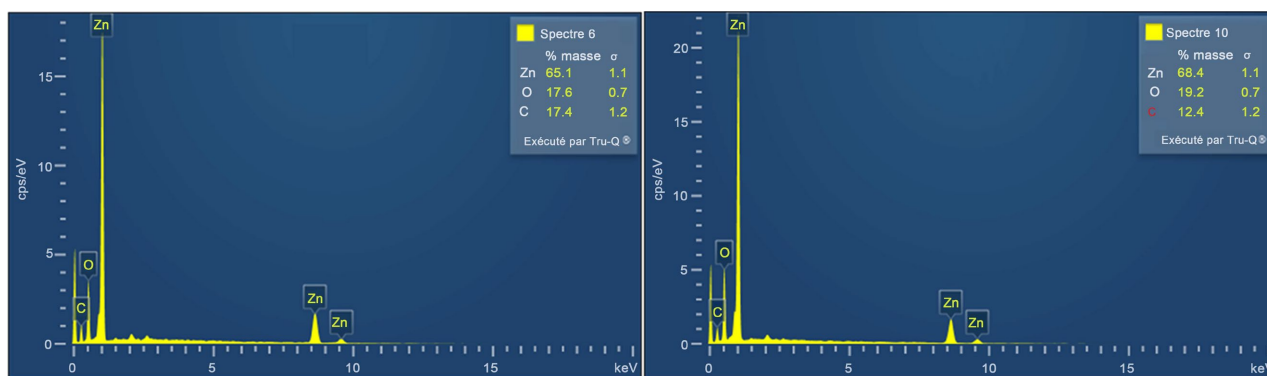
Figure 4. Field emission scanning electron microscopy images of ZnO nanoparticles obtained by anodizing Zn foil: (a) aggregate view; (b) Nanoparticles on micrometric grains.

In order to identify the element composition of the prepared sample, the EDS analysis is conducted during the FESEM observations. The results are presented in **Figures 5(a)-(c)**.

The energy dispersive spectra from the FESEM-EDS analysis show prominent X-ray energies at 0.592 keV and 1.037 keV, respectively, representing the emissions from the K-shell of oxygen and L-shell of zinc [57] [58]. The additional X-ray energies at 8.44 keV and 9.337 keV are additional emission from $K\alpha$ and $K\beta$ core shells of zinc [59]. These results confirm that the sample prepared by the above method is indeed a ZnO phase.



(a)



(b)

(c)

Figure 5. (a) Field emission scanning electron microscopy images of the localized spots of EDS analysis. (b) (c) Associated EDS spectra related to some of the spotted points of analysis.

3.5. Transmission Electron Microscopy (TEM) Characterizations

Figure 6 shows the TEM images of the synthesized sample. The images confirm the presence of a dual structure of the surface of the powder produced. It is seen that nanoparticles are superimposed on micrometric grains. ZnO nanoparticles have a particle size in the range of 20 - 80 nm, which is in line with previous analyses.

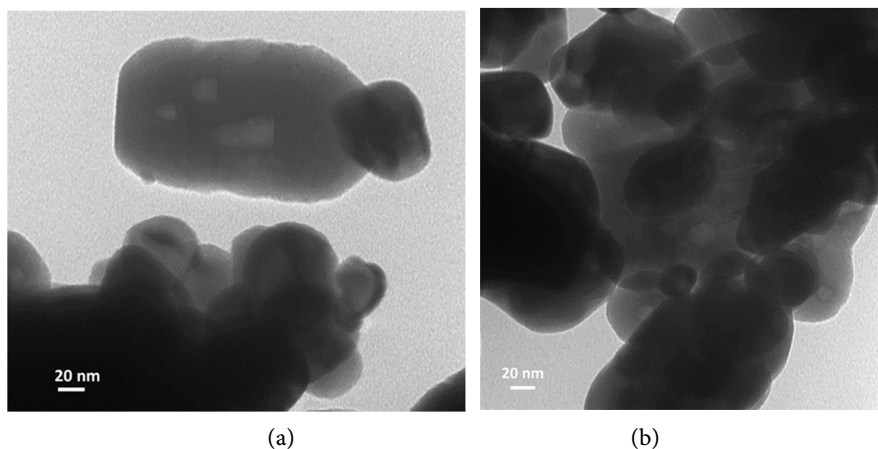


Figure 6. TEM images of ZnO nanoparticles obtained by anodizing Zn foil.

3.6. Ultraviolet-Visible Analysis

The optical absorption spectrum of the synthesized ZnO nanoparticles is shown in **Figure 7**. The used sample is made by dispersion of a small amount of ZnO nanoparticles in deionized water. A sharp absorbance peak is found at 374 nm, which is in good agreement with published studies [60] [61] and confirms the presence of ZnO nanoparticles in the aqueous solution.

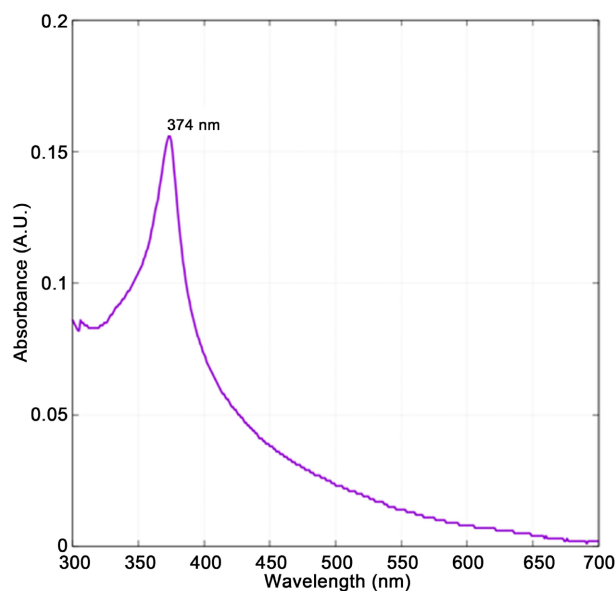


Figure 7. UV-vis absorbance spectrum of ZnO nanoparticles obtained by anodizing Zn foil.

The energy band gap is determined using the recorded UV-Visible data. Using the Tauc equation [62] [63], the plot of $(\alpha h\nu)^2$ versus photon energy ($h\nu$) is presented in **Figure 8**. The intersection of the tangent of the curve with the horizontal energy axis leads to an estimation of the ZnO nanoparticles' energy band gap.

Here the empiric band gap is found to be around 3.17 eV. This value is slightly

lower than the bulk ZnO (3.3 eV) reported in the literature [64] [65].

3.7. Photocatalytic Degradation of Acid Orange 7 Study Using ZnO Nanoparticles

Figure 9 shows typical UV-vis spectra obtained during UV irradiation of AO7 in the presence of ZnO nanoparticles. These spectra clearly show that the intensity of the characteristic band of AO7 at 486 nm decreases as a function of irradiation time. The ZnO nanoparticles are acting as photocatalyst in the degradation reaction of the AO7 dye. After 2 hours of irradiation, the degradation of the dye is significant as attested by **Figure 10**. With a low power density (48 W), a strong photoactivity is recorded.

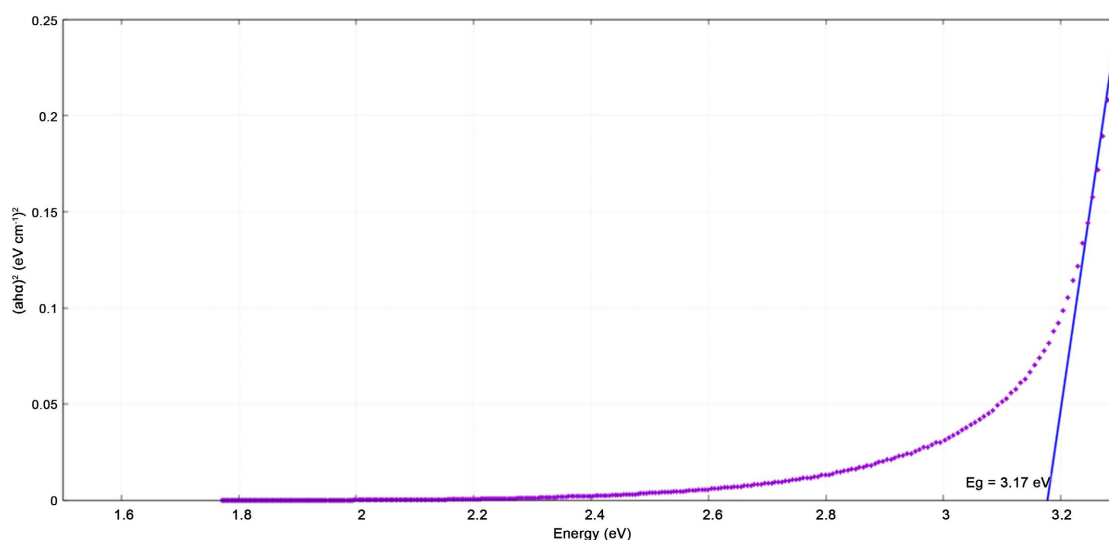


Figure 8. Tauc plot of ZnO nanoparticles obtained by anodizing Zn foil in aqueous dispersion.

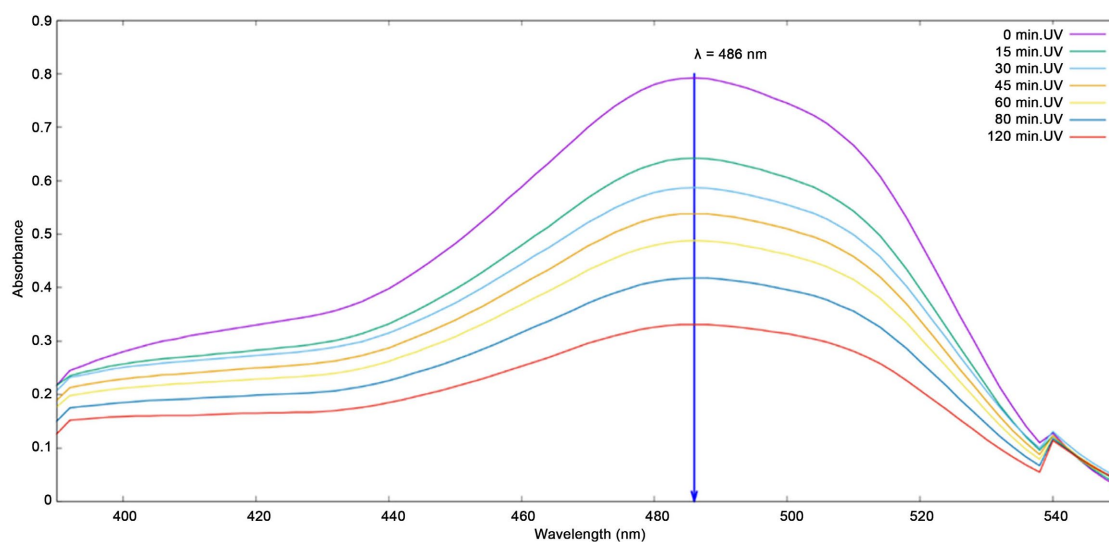


Figure 9. Absorption versus irradiation time for the acid orange 7 (AO7) for polychromatic light (350 - 400 nm) in the presence of ZnO nanoparticles obtained by anodizing Zn foil with exposure times of 0 min, 15 min, 30 min, 45 min, 60 min, 80 min and 120 min.

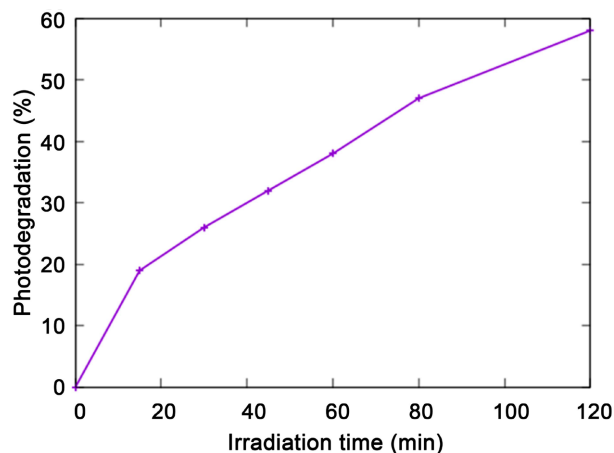


Figure 10. Percentage degradation of AO7 dye mixed with ZnO nanoparticles obtained by anodizing Zn foil.

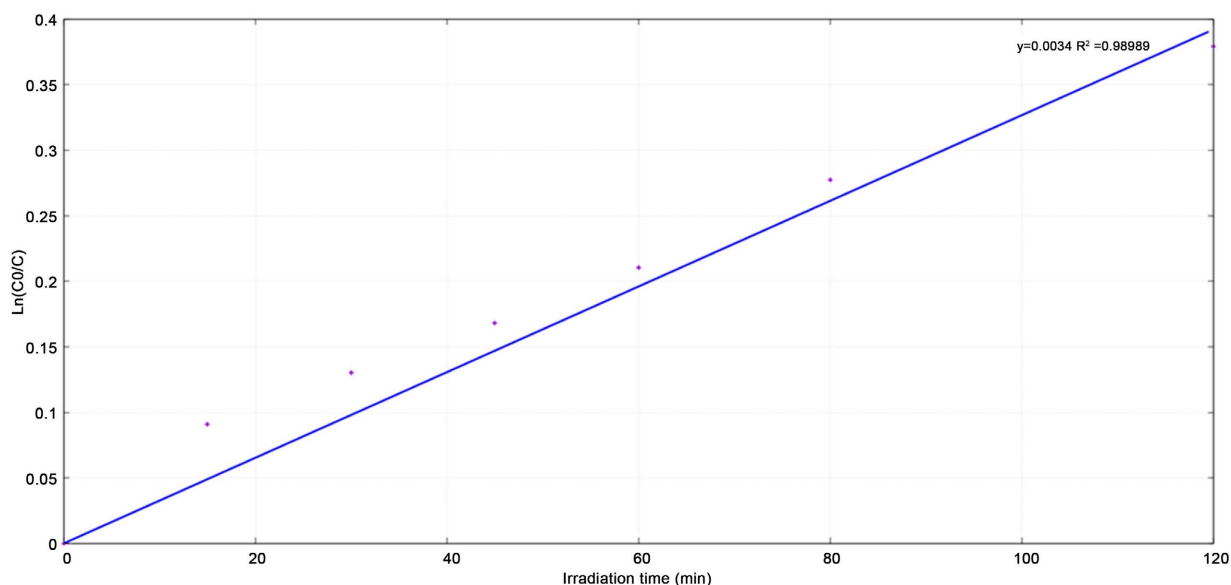


Figure 11. Kinetic curve $\ln(C_0/C) = f(t)$ for the photodegradation of AO7 dye using ZnO nanoparticles obtained by anodizing Zn foil as catalyst.

The kinetic behavior of the photodegradation of AO7 using ZnO nanoparticles as catalyst is studied by plotting $\ln(C_0/C)$ versus t , where C_0 is the initial concentration of AO7 dye and C is AO7 concentration at irradiation time “ t ” see **Figure 11**. A quasi-linear plot between $\ln(C_0/C)$ and the irradiation time is obtained, which describes a pseudo-first-order kinetic reaction for the degradation of AO7 using ZnO NP as photocatalyst [66]. The slope of the line passing through origin determines the rate constant K . The K value and half-time life are found to be 0.0034 min^{-1} and 204 min respectively. The incident light on the surface of ZnO NP creates electron-hole pairs through oxidation reduction reactions which induce radical production in the presence of dioxygen [67]. Hydroxyl and superoxide radicals are of primary importance in the photodegradation of AO7 dye [68]. Oxygen vacancies in ZnO nanoparticles contribute to the photoreaction efficiency

by limiting electron-hole recombination [69]-[71]. The aggregated state of the powder allows rapid natural settling, facilitating the first stage of separation from the supernatant and opening the possibility of reusability of our synthesized ZnO catalysts after an efficient cleaning procedure to desorb undesirable adsorbed by-products.

4. Conclusion

An innovative approach involving an anodization set-up is used to produce ZnO nanopowder. In this process, a large amount of ZnO is synthesized from a Zn sacrificial anode rod at room temperature without any post-treatment. X-ray diffraction reveals the hexagonal zincite-type crystallite of the sample, whereas the FESEM/EDS confirms the morphology and elemental composition of the powder. The produced material is tested to investigate its photocatalytic properties in regard to the kinetic degradation of a model organic dye AO7. Despite the highly aggregated state of the powder, a significant catalytic property is recorded. The dual morphology of nanometric structures superimposed on microscopic grains revealed by FESEM/TEM analysis contributes to an increase in specific surface area, which is conducive to the material's photocatalytic activity. This original synthesis process stands out from others thanks to its ease of use, modularity and low cost, which will enable industrial applications by building a pilot reactor capable of producing ZnO nanoparticles rapidly and in large quantities. This original synthesis process stands out from others thanks to its ease of use, modularity and low cost, which will enable industrial applications by building a pilot reactor capable of producing ZnO nanoparticles rapidly and in large quantities with minor adaptations relating to scale.

Acknowledgements

We would like to thank the Institut Universitaire de Technologie Clermont Auvergne for hosting our laboratory and the Clermont Auvergne Physics Laboratory for financing this work.

Conflicts of Interest

The authors declare no conflicts of interest regarding the publication of this paper.

References

- [1] Kreuter, J. and Speiser, P.P. (1976) *In Vitro* Studies of Poly(Methyl Methacrylate) Adjuvants. *Journal of Pharmaceutical Sciences*, **65**, 1624-1627. <https://doi.org/10.1002/jps.2600651115>
- [2] Gottardo, S., Mech, A., Drbohlavová, J., Malyska, A., Bøwadt, S., Riego Sintes, J., *et al.* (2021) Towards Safe and Sustainable Innovation in Nanotechnology: State-Of-Play for Smart Nanomaterials. *NanoImpact*, **21**, Article ID: 100297. <https://doi.org/10.1016/j.impact.2021.100297>
- [3] Bhushan, B. (2017) Springer Handbook of Nanotechnology. Springer. <https://doi.org/10.1007/978-3-662-54357-3>

- [4] Rotello, V. (2004) Nanoparticles: Building Blocks for Nanotechnology. Springer. <https://doi.org/10.1007/978-1-4419-9042-6>
- [5] Petros, R.A. and DeSimone, J.M. (2010) Strategies in the Design of Nanoparticles for Therapeutic Applications. *Nature Reviews Drug Discovery*, **9**, 615-627. <https://doi.org/10.1038/nrd2591>
- [6] Salata, O. (2004) Applications of Nanoparticles in Biology and Medicine. *Journal of Nanobiotechnology*, **2**, Article No. 3. <https://doi.org/10.1186/1477-3155-2-3>
- [7] Stark, W.J., Stoessel, P.R., Wohlleben, W. and Hafner, A. (2015) Industrial Applications of Nanoparticles. *Chemical Society Reviews*, **44**, 5793-5805. <https://doi.org/10.1039/c4cs00362d>
- [8] Santos, C.S.C., Gabriel, B., Blanchy, M., Menes, O., García, D., Blanco, M., *et al.* (2015) Industrial Applications of Nanoparticles—A Prospective Overview. *Materials Today: Proceedings*, **2**, 456-465. <https://doi.org/10.1016/j.matpr.2015.04.056>
- [9] Schmid, K. and Riediker, M. (2008) Use of Nanoparticles in Swiss Industry: A Targeted Survey. *Environmental Science & Technology*, **42**, 2253-2260. <https://doi.org/10.1021/es071818o>
- [10] Panpatte, D.G., Jhala, Y.K., Shelat, H.N. and Vyas, R.V. (2016) Nanoparticles: The Next Generation Technology for Sustainable Agriculture. In: Singh, D., Singh, H. and Prabha, R., Eds., *Microbial Inoculants in Sustainable Agricultural Productivity*, Springer, 289-300. https://doi.org/10.1007/978-81-322-2644-4_18
- [11] Singh, R.P., Handa, R. and Manchanda, G. (2021) Nanoparticles in Sustainable Agriculture: An Emerging Opportunity. *Journal of Controlled Release*, **329**, 1234-1248. <https://doi.org/10.1016/j.jconrel.2020.10.051>
- [12] Tang, S.C.N. and Lo, I.M.C. (2013) Magnetic Nanoparticles: Essential Factors for Sustainable Environmental Applications. *Water Research*, **47**, 2613-2632. <https://doi.org/10.1016/j.watres.2013.02.039>
- [13] Thomas, J., Myara, M., Troussellier, L., Burov, E., Pastouret, A., Boivin, D., *et al.* (2012) Radiation-Resistant Erbium-Doped-Nanoparticles Optical Fiber for Space Applications. *Optics Express*, **20**, 2435-2444. <https://doi.org/10.1364/oe.20.002435>
- [14] Marciano, F.R., Bonetti, L.F., Pessoa, R.S., Marcuzzo, J.S., Massi, M., Santos, L.V., *et al.* (2008) The Improvement of DLC Film Lifetime Using Silver Nanoparticles for Use on Space Devices. *Diamond and Related Materials*, **17**, 1674-1679. <https://doi.org/10.1016/j.diamond.2008.03.007>
- [15] Fu, X., Cai, J., Zhang, X., Li, W., Ge, H. and Hu, Y. (2018) Top-Down Fabrication of Shape-Controlled, Monodisperse Nanoparticles for Biomedical Applications. *Advanced Drug Delivery Reviews*, **132**, 169-187. <https://doi.org/10.1016/j.addr.2018.07.006>
- [16] Abid, N., Khan, A.M., Shujait, S., Chaudhary, K., Ikram, M., Imran, M., *et al.* (2022) Synthesis of Nanomaterials Using Various Top-Down and Bottom-Up Approaches, Influencing Factors, Advantages, and Disadvantages: A Review. *Advances in Colloid and Interface Science*, **300**, Article ID: 102597. <https://doi.org/10.1016/j.cis.2021.102597>
- [17] Djurišić, A.B., Ng, A.M.C. and Chen, X.Y. (2010) ZnO Nanostructures for Optoelectronics: Material Properties and Device Applications. *Progress in Quantum Electronics*, **34**, 191-259. <https://doi.org/10.1016/j.pquantelec.2010.04.001>
- [18] Belhaj, M., Dridi, C., Elhouichet, H. and Valmalette, J.C. (2016) Study of ZnO Nanoparticles Based Hybrid Nanocomposites for Optoelectronic Applications. *Journal of Applied Physics*, **119**, Article ID: 095501. <https://doi.org/10.1063/1.4942525>

- [19] Muchuweni, E., Sathiaraj, T.S. and Nyakoty, H. (2017) Synthesis and Characterization of Zinc Oxide Thin Films for Optoelectronic Applications. *Heliyon*, **3**, e00285. <https://doi.org/10.1016/j.heliyon.2017.e00285>
- [20] Wong, K.K., Ng, A., Chen, X.Y., Ng, Y.H., Leung, Y.H., Ho, K.H., *et al.* (2012) Effect of ZnO Nanoparticle Properties on Dye-Sensitized Solar Cell Performance. *ACS Applied Materials & Interfaces*, **4**, 1254-1261. <https://doi.org/10.1021/am201424d>
- [21] Shashanka, R., Esgin, H., Yilmaz, V.M. and Caglar, Y. (2020) Fabrication and Characterization of Green Synthesized ZnO Nanoparticle Based Dye-Sensitized Solar Cells. *Journal of Science: Advanced Materials and Devices*, **5**, 185-191. <https://doi.org/10.1016/j.jsamd.2020.04.005>
- [22] Elkhidir Suliman, A., Tang, Y. and Xu, L. (2007) Preparation of ZnO Nanoparticles and Nanosheets and Their Application to Dye-Sensitized Solar Cells. *Solar Energy Materials and Solar Cells*, **91**, 1658-1662. <https://doi.org/10.1016/j.solmat.2007.05.014>
- [23] Kahouli, M., Barhoumi, A., Bouzid, A., Al-Hajry, A. and Guermazi, S. (2015) Structural and Optical Properties of ZnO Nanoparticles Prepared by Direct Precipitation Method. *Superlattices and Microstructures*, **85**, 7-23. <https://doi.org/10.1016/j.spmi.2015.05.007>
- [24] Raoufi, D. (2013) Synthesis and Microstructural Properties of ZnO Nanoparticles Prepared by Precipitation Method. *Renewable Energy*, **50**, 932-937. <https://doi.org/10.1016/j.renene.2012.08.076>
- [25] An, L.J., Wang, J., Zhang, T.F., Yang, H.L. and Sun, Z.H. (2011) Synthesis of ZnO Nanoparticles by Direct Precipitation Method. *Advanced Materials Research*, **380**, 335-338. <https://doi.org/10.4028/www.scientific.net/amr.380.335>
- [26] Manikandan, B., Endo, T., Kaneko, S., Murali, K.R. and John, R. (2018) Properties of Sol Gel Synthesized ZnO Nanoparticles. *Journal of Materials Science: Materials in Electronics*, **29**, 9474-9485. <https://doi.org/10.1007/s10854-018-8981-8>
- [27] Hasnidawani, J.N., Azlina, H.N., Norita, H., Bonnia, N.N., Ratim, S. and Ali, E.S. (2016) Synthesis of ZnO Nanostructures Using Sol-Gel Method. *Procedia Chemistry*, **19**, 211-216. <https://doi.org/10.1016/j.proche.2016.03.095>
- [28] Chung, Y.T., Ba-Abbad, M.M., Mohammad, A.W., Hairom, N.H.H. and Benamor, A. (2015) Synthesis of Minimal-Size ZnO Nanoparticles through Sol-Gel Method: Taguchi Design Optimisation. *Materials & Design*, **87**, 780-787. <https://doi.org/10.1016/j.matdes.2015.07.040>
- [29] Aneesh, P.M., Vanaja, K.A. and Jayaraj, M.K. (2007) Synthesis of ZnO Nanoparticles by Hydrothermal Method. *SPIE Proceedings*, **6639**. <https://doi.org/10.1117/12.730364>
- [30] Bharti, D.B. and Bharati, A.V. (2016) Synthesis of ZnO Nanoparticles Using a Hydrothermal Method and a Study Its Optical Activity. *Luminescence*, **32**, 317-320. <https://doi.org/10.1002/bio.3180>
- [31] Kumaresan, N., Ramamurthi, K., Ramesh Babu, R., Sethuraman, K. and Moorthy Babu, S. (2017) Hydrothermally Grown ZnO Nanoparticles for Effective Photocatalytic Activity. *Applied Surface Science*, **418**, 138-146. <https://doi.org/10.1016/j.apsusc.2016.12.231>
- [32] Lee, G.J., Choi, E.H., Nam, S., Lee, J.S., Boo, J., Oh, S.D., *et al.* (2019) Optical Sensing Properties of ZnO Nanoparticles Prepared by Spray Pyrolysis. *Journal of Nanoscience and Nanotechnology*, **19**, 1048-1051. <https://doi.org/10.1166/jnn.2019.15918>
- [33] Lee, S.D., Nam, S., Kim, M. and Boo, J. (2012) Synthesis and Photocatalytic Property

- of ZnO Nanoparticles Prepared by Spray-Pyrolysis Method. *Physics Procedia*, **32**, 320-326. <https://doi.org/10.1016/j.phpro.2012.03.563>
- [34] Wallace, R., Brown, A.P., Brydson, R., Wegner, K. and Milne, S.J. (2013) Synthesis of ZnO Nanoparticles by Flame Spray Pyrolysis and Characterisation Protocol. *Journal of Materials Science*, **48**, 6393-6403. <https://doi.org/10.1007/s10853-013-7439-x>
- [35] Umar, A., Kumar, R., Kumar, G., Algarni, H. and Kim, S.H. (2015) Effect of Annealing Temperature on the Properties and Photocatalytic Efficiencies of ZnO Nanoparticles. *Journal of Alloys and Compounds*, **648**, 46-52. <https://doi.org/10.1016/j.jallcom.2015.04.236>
- [36] El-Desoky, M.M., Ali, M.A., Afifi, G., Imam, H. and Al-Assiri, M.S. (2016) Effects of Annealing Temperatures on the Structural and Dielectric Properties of ZnO Nanoparticles. *Silicon*, **10**, 301-307. <https://doi.org/10.1007/s12633-016-9445-5>
- [37] Omri, K., Najeh, I. and El Mir, L. (2016) Influence of Annealing Temperature on the Microstructure and Dielectric Properties of ZnO Nanoparticles. *Ceramics International*, **42**, 8940-8948. <https://doi.org/10.1016/j.ceramint.2016.02.151>
- [38] Minagar, S., Berndt, C.C., Wang, J., Ivanova, E. and Wen, C. (2012) A Review of the Application of Anodization for the Fabrication of Nanotubes on Metal Implant Surfaces. *Acta Biomaterialia*, **8**, 2875-2888. <https://doi.org/10.1016/j.actbio.2012.04.005>
- [39] Fukuda, H. and Matsumoto, Y. (2004) Effects of Na₂SiO₃ on Anodization of Mg-Al-Zn Alloy in 3 M KOH Solution. *Corrosion Science*, **46**, 2135-2142. <https://doi.org/10.1016/j.corsci.2004.02.001>
- [40] Kulkarni, M., Mazare, A., Schmuki, P. and Igljic, A. (2016) Influence of Anodization Parameters on Morphology of TiO₂ Nanostructured Surfaces. *Advanced Materials Letters*, **7**, 23-28. <https://doi.org/10.5185/amlett.2016.6156>
- [41] Sulka, G.D. (2020) Introduction to Anodization of Metals. In: Sulka, G.D., Ed., *Nanostructured Anodic Metal Oxides*, Elsevier, 1-34. <https://doi.org/10.1016/b978-0-12-816706-9.00001-7>
- [42] Robinson Aguirre, O. and Félix Echeverría, E. (2018) Effects of Fluoride Source on the Characteristics of Titanium Dioxide Nanotubes. *Applied Surface Science*, **445**, 308-319. <https://doi.org/10.1016/j.apsusc.2018.03.139>
- [43] İzmir, M. and Ercan, B. (2018) Anodization of Titanium Alloys for Orthopedic Applications. *Frontiers of Chemical Science and Engineering*, **13**, 28-45. <https://doi.org/10.1007/s11705-018-1759-y>
- [44] Kim, S.J., Lee, J. and Choi, J. (2008) Understanding of Anodization of Zinc in an Electrolyte Containing Fluoride Ions. *Electrochimica Acta*, **53**, 7941-7945. <https://doi.org/10.1016/j.electacta.2008.06.006>
- [45] Kuan, C.Y., Chou, J.M., Leu, I.C. and Hon, M.H. (2007) Formation and Field Emission Property of Single-Crystalline Zn Microtip Arrays by Anodization. *Electrochemistry Communications*, **9**, 2093-2097. <https://doi.org/10.1016/j.elecom.2007.06.004>
- [46] Shetty, A. and Nanda, K.K. (2012) Synthesis of Zinc Oxide Porous Structures by Anodization with Water as an Electrolyte. *Applied Physics A*, **109**, 151-157. <https://doi.org/10.1007/s00339-012-7023-2>
- [47] Elam, J.W. and George, S.M. (2003) Growth of ZnO/Al₂O₃ Alloy Films Using Atomic Layer Deposition Techniques. *Chemistry of Materials*, **15**, 1020-1028.
- [48] Hynes, A.P., Doremus, R.H. and Siegel, R.W. (2002) Sintering and Characterization of Nanophase Zinc Oxide. *Journal of the American Ceramic Society*, **85**, 1979-1987. <https://doi.org/10.1111/j.1151-2916.2002.tb00391.x>
- [49] Mahian, O., Kianifar, A. and Wongwises, S. (2013) Dispersion of ZnO Nanoparticles

- in a Mixture of Ethylene Glycol-Water, Exploration of Temperature-Dependent Density, and Sensitivity Analysis. *Journal of Cluster Science*, **24**, 1103-1114. <https://doi.org/10.1007/s10876-013-0601-4>
- [50] Xu, F., Zhang, P., Navrotsky, A., Yuan, Z., Ren, T., Halasa, M., *et al.* (2007) Hierarchically Assembled Porous ZnO Nanoparticles: Synthesis, Surface Energy, and Photocatalytic Activity. *Chemistry of Materials*, **19**, 5680-5686. <https://doi.org/10.1021/cm071190g>
- [51] Radovanovic, P.V., Norberg, N.S., McNally, K.E. and Gamelin, D.R. (2002) Colloidal Transition-Metal-Doped ZnO Quantum Dots. *Journal of the American Chemical Society*, **124**, 15192-15193. <https://doi.org/10.1021/ja028416v>
- [52] Wu, Y.L., Lim, C.S., Fu, S., Tok, A.I.Y., Lau, H.M., Boey, F.Y.C., *et al.* (2007) Surface Modifications of ZnO Quantum Dots for Bio-Imaging. *Nanotechnology*, **18**, Article ID: 215604. <https://doi.org/10.1088/0957-4484/18/21/215604>
- [53] Flores, N.M., Pal, U., Galeazzi, R. and Sandoval, A. (2014) Effects of Morphology, Surface Area, and Defect Content on the Photocatalytic Dye Degradation Performance of ZnO Nanostructures. *RSC Advances*, **4**, 41099-41110. <https://doi.org/10.1039/c4ra04522j>
- [54] Yamamoto, O., Hotta, M., Sawai, J., Sasamoto, T. and Kojima, H. (1998) Influence of Powder Characteristic of ZnO on Antibacterial Activity. *Journal of the Ceramic Society of Japan*, **106**, 1007-1011. <https://doi.org/10.2109/jcersj.106.1007>
- [55] Mateos-Pedrero, C., Silva, H., Pacheco Tanaka, D.A., Liguori, S., Iulianelli, A., Basile, A., *et al.* (2015) CuO/ZnO Catalysts for Methanol Steam Reforming: The Role of the Support Polarity Ratio and Surface Area. *Applied Catalysis B: Environment and Energy*, **174**, 67-76. <https://doi.org/10.1016/j.apcatb.2015.02.039>
- [56] Sun, Y., Chen, L., Bao, Y., Zhang, Y., Wang, J., Fu, M., *et al.* (2016) The Applications of Morphology Controlled ZnO in Catalysis. *Catalysts*, **6**, Article 188. <https://doi.org/10.3390/catal6120188>
- [57] Uma, K., Ananthakumar, S., Mangalaraja, R.V., Mahesh, K.P.O., Soga, T. and Jimbo, T. (2008) A Facile Approach to Hexagonal ZnO Nanorod Assembly. *Journal of Sol-Gel Science and Technology*, **49**, 1-5. <https://doi.org/10.1007/s10971-008-1846-5>
- [58] Bin, Z., Liu, Z., Qiu, Y. and Duan, L. (2018) Efficient N-Dopants and Their Roles in Organic Electronics. *Advanced Optical Materials*, **6**, Article ID: 1800536. <https://doi.org/10.1002/adom.201800536>
- [59] Velumani, S. and Ascencio, J.A. (2004) Formation of ZnS Nanorods by Simple Evaporation Technique. *Applied Physics A*, **79**, 153-156. <https://doi.org/10.1007/s00339-003-2367-2>
- [60] Singh, S., Gade, J.V., Verma, D.K., Elyor, B. and Jain, B. (2024) Exploring ZnO Nanoparticles: UV-Visible Analysis and Different Size Estimation Methods. *Optical Materials*, **152**, 115422. <https://doi.org/10.1016/j.optmat.2024.115422>
- [61] Muhammad, W., Ullah, N., Haroon, M. and Abbasi, B.H. (2019) Optical, Morphological and Biological Analysis of Zinc Oxide Nanoparticles (ZnO NpS) Using *Papaver somniferum* L. *RSC Advances*, **9**, 29541-29548. <https://doi.org/10.1039/c9ra04424h>
- [62] Haryński, Ł., Olejnik, A., Grochowska, K. and Siuzdak, K. (2022) A Facile Method for Tauc Exponent and Corresponding Electronic Transitions Determination in Semiconductors Directly from UV-Vis Spectroscopy Data. *Optical Materials*, **127**, Article ID: 112205. <https://doi.org/10.1016/j.optmat.2022.112205>
- [63] Jubu, P.R., Yam, F.K., Igba, V.M. and Beh, K.P. (2020) Tauc-Plot Scale and Extrapolation

- lation Effect on Bandgap Estimation from UV-vis-NIR Data—A Case Study of β -Ga₂O₃. *Journal of Solid State Chemistry*, **290**, Article ID: 121576. <https://doi.org/10.1016/j.jssc.2020.121576>
- [64] Shan, F.K. and Yu, Y.S. (2004) Band Gap Energy of Pure and Al-Doped ZnO Thin Films. *Journal of the European Ceramic Society*, **24**, 1869-1872. [https://doi.org/10.1016/s0955-2219\(03\)00490-4](https://doi.org/10.1016/s0955-2219(03)00490-4)
- [65] Zeuner, A., Alves, H., Hofmann, D.M., Meyer, B.K., Heuken, M., Bläsing, J., *et al.* (2002) Structural and Optical Properties of Epitaxial and Bulk ZnO. *Applied Physics Letters*, **80**, 2078-2080. <https://doi.org/10.1063/1.1464218>
- [66] Baran, W., Adamek, E. and Makowski, A. (2008) The Influence of Selected Parameters on the Photocatalytic Degradation of Azo-Dyes in the Presence of TiO₂ Aqueous Suspension. *Chemical Engineering Journal*, **145**, 242-248. <https://doi.org/10.1016/j.cej.2008.04.021>
- [67] Ong, C.B., Ng, L.Y. and Mohammad, A.W. (2018) A Review of ZnO Nanoparticles as Solar Photocatalysts: Synthesis, Mechanisms and Applications. *Renewable and Sustainable Energy Reviews*, **81**, 536-551. <https://doi.org/10.1016/j.rser.2017.08.020>
- [68] Sang, Y., Li, J., Zhou, J., Li, Y., Zhang, J., Xia, X., *et al.* (2024) The Activation of Peroxymonosulfate via Oxygen/Cobalt-Modified Carbon Nitride for Decomposition of Acid Orange 7: Role of High-Value Cobalt and Superoxide Radical. *Research on Chemical Intermediates*, **50**, 4155-4174. <https://doi.org/10.1007/s11164-024-05364-9>
- [69] Janotti, A. and Van de Walle, C.G. (2005) Oxygen Vacancies in ZnO. *Applied Physics Letters*, **87**, Article ID: 122102. <https://doi.org/10.1063/1.2053360>
- [70] Leiter, F., Alves, H., Pfisterer, D., Romanov, N.G., Hofmann, D.M. and Meyer, B.K. (2003) Oxygen Vacancies in ZnO. *Physica B: Condensed Matter*, **340**, 201-204. <https://doi.org/10.1016/j.physb.2003.09.031>
- [71] Hofmann, D.M., Pfisterer, D., Sann, J., Meyer, B.K., Tena-Zaera, R., Munoz-Sanjose, V., *et al.* (2007) Properties of the Oxygen Vacancy in ZnO. *Applied Physics A*, **88**, 147-151. <https://doi.org/10.1007/s00339-007-3956-2>